Complex modes expansion with vector projection using power flow to simulate Lamb waves scattering from horizontal cracks and disbonds

Banibrata Poddar[a] and Victor Giurgiutiu
Department of Mechanical Engineering, University of South Carolina, Columbia, South Carolina 29208, USA

(Received 30 March 2016; revised 2 August 2016; accepted 7 September 2016; published online 29 September 2016)

This paper presents an inexpensive but accurate analytical method to calculate the scattering of straight-crested Lamb waves from cracks parallel to the plate surface. The same method is applicable for the disbond problem. In this method, the scatter field is expanded in terms of complex Lamb wave modes with unknown amplitudes. These unknown amplitudes are obtained from the boundary conditions using vector projection utilizing the power expression. The process works by projecting the stress conditions onto the displacement eigen-spaces of complex Lamb wave modes and vice versa. The authors call this technique "complex modes expansion with vector projection" (CMEP). The CMEP approach is versatile and can be readily applied to corrosion, cracks, or disbonds. In this paper, the CMEP method is applied to a horizontal crack in a plate. For verification of the results the authors compared them with the results obtained by using the finite element method (FEM) and literature. The FEM analysis was conducted in the frequency domain with non-reflecting boundaries. It was found that CMEP results correspond very well with FEM results over a wide frequency-thickness range up to 1.5 MHz mm with CMEP being orders of magnitude faster than FEM. © *2016 Acoustical Society of America*.
[http://dx.doi.org/10.1121/1.4963087]

[AJH] Pages: 2123–2133

I. INTRODUCTION

Lamb waves are capable of inspecting large structures for non-destructive evaluation (NDE) and structural health monitoring (SHM) because they travel long distances without much attenuation. Therefore, interaction of Lamb waves with damage has been an important topic of research. In particular, the interaction with horizontal cracks is important not only in the case of disbonds in layered media, but also in the case of forging and diffusion bonding of isotropic materials (Lampman *et al.*, 1992). However, the detection and characterization of damage using Lamb wave propagation involves a difficult inverse problem which requires fast and accurate prediction of the scattered waves. But, the prediction of the scattered waves is highly challenging because of the existence of multiple dispersive modes of Lamb waves at any frequency along with mode conversion at the damage location. Therefore, well-developed numerical methods such as the finite element method (FEM) and the boundary element method (BEM) have been popular (Cho and Rose, 2000; Galán and Abascal, 2005; Mackerle, 2004; Moser *et al.*, 1999). However, commercial FEM codes are time consuming and they do not provide much insight of the wave field in the structure, especially near the damage location. Therefore, for efficiency of simulation, researchers have developed hybrid methods using FEM, BEM, and normal mode expansion (Cho and Rose, 2000; Galán and Abascal, 2005; Gunawan and Hirose, 2004; Terrien *et al.*, 2007). For interaction with horizontal cracks, Karim *et al.* (1992) and Gunawan and Hirose (2004) combined FEM with analytical approach for faster prediction of the scatter field of Lamb waves. Full analytical approaches such as the Wiener-Hopf technique and higher order plate theories were also used by Rocklin (1980) and Wang and Rose (2003) to solve this problem. Glushkov *et al.* (2009) have proposed the layered element method which, unlike BEM, satisfies the plate boundary conditions by formulation. However, the prospect of developing full analytical models based on normal mode expansion has also attracted attention for possible speed and accuracy (Castaings *et al.*, 2002; Flores-López and Gregory, 2006; Grahn, 2003; Gregory and Gladwell, 1983; Moreau *et al.*, 2011, 2012; Torvik, 1966).

For problems of guided waves encountering changing boundary conditions such as stiffeners, Hull and Maguire (2014) and Hull and Welch (2010) have used modal expansion with unknown wave propagation coefficients. They used orthogonalization to obtain a set of linear equations to solve for unknown coefficients. One of the main challenges of such a method is to satisfy the thickness dependent boundary conditions (Castaings *et al.*, 2002; Terrien *et al.*, 2007). Gregory and Gladwell (1982, 1983) developed the "projection method" to satisfy these continuous boundary conditions. This method was developed to predict the singularity in stresses in the case of geometric discontinuities (Flores-López and Gregory, 2006). A scalar form of the projection method was also used by Grahn (2003); though simple, this proved not to be very stable and to have slow convergence due to the use of simple sine and cosine functions (Moreau *et al.*, 2012). Moreau *et al.* (2011) used the

[a]Electronic mail: poddarb@email.sc.edu

displacement components of the complex Lamb wave modeshapes instead of simple sine and cosine functions and attained a faster convergence in the projection method.

In this paper, we present an efficient analytical method for the prediction of Lamb wave scatter field using complex mode expansion and vector projection. We improved in several ways upon previous authors. One improvement is that we modified the projection method to take advantage of the power flow associated with Lamb wave modes. As different from Grahn (2003) and Moreau *et al.* (2011), the stress boundary conditions are projected onto the conjugate of the displacement modeshapes and the displacement boundary conditions are projected onto the conjugate of the stress modeshapes. Therefore, this method transforms the stress and displacement equations into power equations. As mentioned by Moreau *et al.* (2012), this type of approach creates diagonally dominant matrices with more zeros to be inverted. We used this projection method to incorporate power flow associated with all the unknown wave fields leading to fast convergence in time. This approach automatically ensures the power balance when the method has converged. We call this method complex modes expansion with vector projection (CMEP). This is a Galerkin type approach where we implemented vector projection of the boundary conditions directly using the power flow expression. We illustrate the CMEP method by applying it to the case of a horizontal crack.

The paper is organized as follows: Section II describes the CMEP method using the horizontal crack problem; Sec. III verifies CMEP results by comparing them with the results from finite element models over a large range of frequencies; and finally, Sec. IV contains a summary and conclusion of the presented work along with future work.

II. ANALYTICAL MODEL FOR LAMB WAVES SCATTERING

A. Straight crested Lamb waves in a plate

Lamb waves are plate guided waves with multiple propagating modes at any given frequency. The characteristic equation of Lamb waves known as the Rayleigh-Lamb Equation (Lamb, 1917) in dimensionless form, $K = \xi d$ is the dimensionless wavenumber, and $\Omega = \omega d/c_S$ is the dimensionless frequency

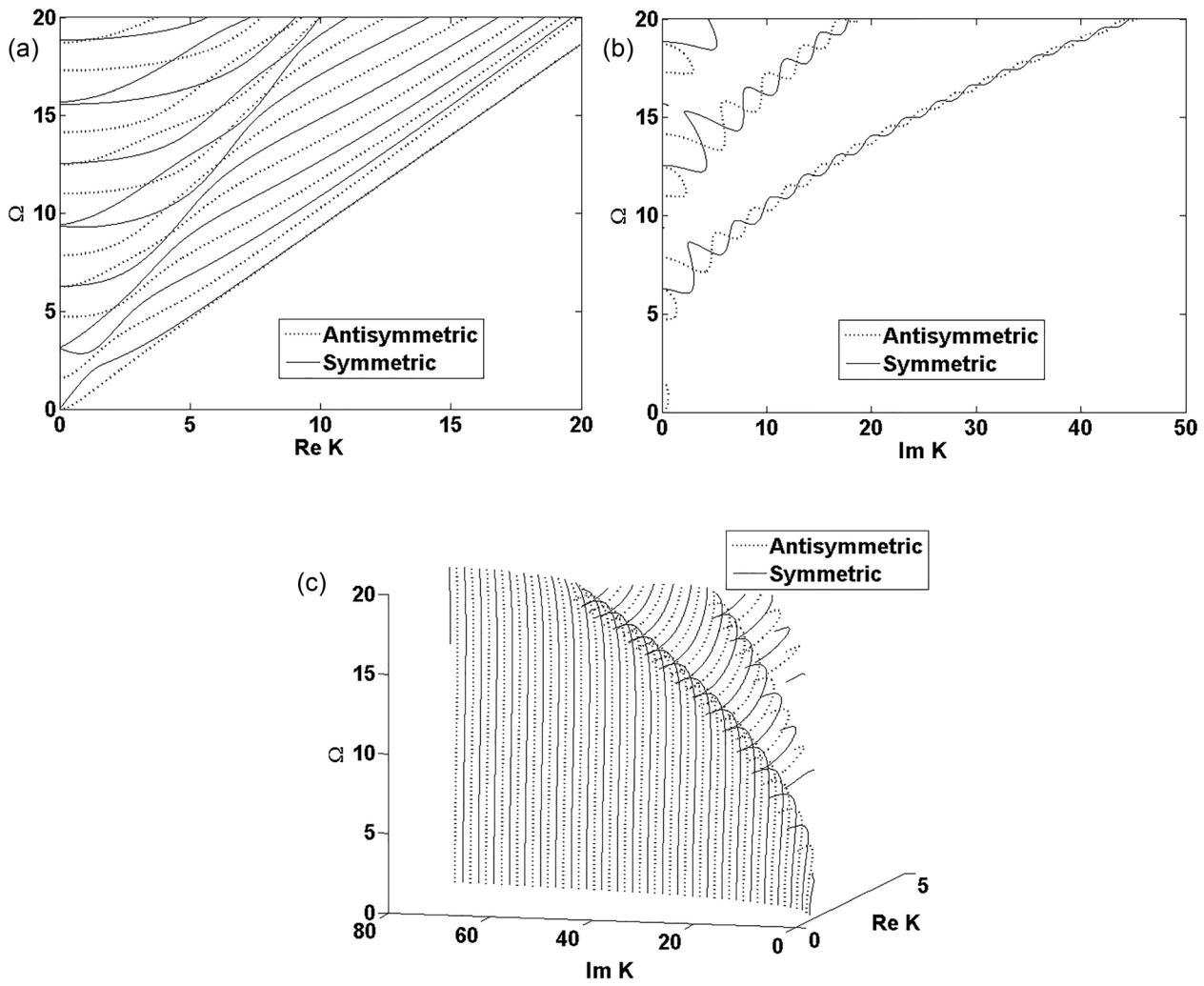

FIG. 1. (a) Real, (b) imaginary, and (c) complex roots of the Rayleigh-Lamb equation for $\nu = 0.33$.

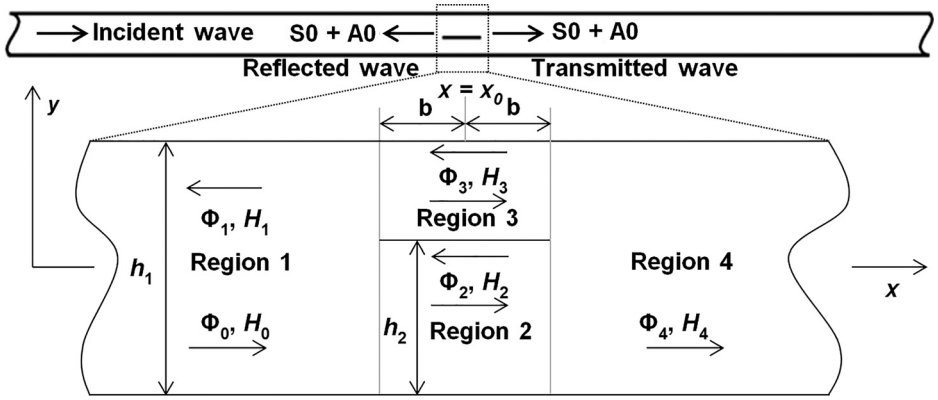

FIG. 2. Schematic of Lamb waves interacting with a horizontal crack or disbond.

$$D_S(K,\Omega) = (K^2-a^2)^2 \sin a \cos b + 4abK^2 \cos a \sin b = 0 \quad \text{(Symmetric)},$$
$$D_A(K,\Omega) = (K^2-a^2)^2 \sin b \cos a + 4abK^2 \cos b \sin a = 0 \quad \text{(Antisymmetric)}, \tag{1}$$

where $a = (\Omega^2 - K^2)^{1/2}$, $b = (\Omega^2/\kappa^2 - K^2)^{1/2}$, $\kappa = c_P/c_S$, $d = h/2$ is the half-thickness of the plate. Note that the problem has decoupled into a symmetric case (constants A2 and B1) and an antisymmetric case (constants A1 and B2). The wave motion associated with each root K for given Ω is expressed as

$$F(X,\ Y,\ T) = A(Y)e^{-K_{\text{imag}}X}e^{iK_{\text{real}}X}e^{-i\Omega T};$$
$$K = K_{\text{real}} + iK_{\text{imag}}, \tag{2}$$

where $X = x/d$, $Y = y/d$ are dimensionless propagation direction and thickness direction, respectively, and $T = tc_S/d$ being dimensionless time. At any frequency Ω, Eq. (1) has an infinite number of roots K, $-\bar{K}$, $-K$, and $\bar{K}$ in all four quadrants of the complex plane; a finite number of these roots are real [Fig. 1(a)], a finite number of them are imaginary [Fig. 1(b)], and the remainder are complex roots [Fig. 1(c)]. It is apparent from Eq. (2) that the wave motions associated with these roots are harmonic in both time and space for K being real, harmonic in time and exponentially decaying amplitude in space for K being imaginary, and harmonic in both time and space with exponentially decaying amplitude for K being complex. The positive real roots are assumed to be associated with modes propagating in the positive X direction. Also, for the wave motion to be physically plausible, the positive imaginary roots and the complex roots with positive imaginary parts are assumed to be associated with the positive X direction as they decay exponentially in the positive X direction. It is well known that the scattering of Lamb waves from geometric discontinuities involves all these wave modes in order to satisfy the boundary conditions (Diligent *et al.*, 2003; Morvan *et al.*, 2003). Using a modified bracketing method, we found these roots iteratively and sorted the complex roots with ascending imaginary part (Fig. 1).

B. Setup of the scattering problem

To begin our analysis, let us consider a plate with a cross section as shown in Fig. 2. We assume that there is an incident straight-crested Lamb wave mode traveling from the left toward a disbond in the form of a horizontal crack. Upon interacting with the disbond, it will result in reflected wave modes, transmitted wave modes, and wave modes trapped in the disbond. As shown in Fig. 2, the disbond is located at a distance $x = x_0$ in a plate with thickness h_1. The disbond has a width $L = 2b$ and is located at height h_2 from the bottom of the plate. At the disbond, we define depth ration as $R_d = (h_1 - h_2)/h_1$ and width ratio as $R_w = 2b/h_1$. Also, let us imagine that the incident wave field is represented by $(\Phi_0,\ H_0)$, traveling in $+ve$ x direction in Region 1. We define the reflected wave field as $(\Phi_1,\ H_1)$ and the transmitted wave field in Region 4 as $(\Phi_4,\ H_4)$. We also define the trapped wave field in the disbond area as $(\Phi_2,\ H_2)$ and $(\Phi_3,\ H_3)$ in Regions 2 and 3, respectively. The incident and scattered wave fields satisfy the generic wave equations

$$\frac{\partial^2\Phi}{\partial x^2} + \frac{\partial^2\Phi}{\partial y^2} = \frac{1}{c_P^2}\ddot{\Phi}, \quad \frac{\partial^2 H}{\partial x^2} + \frac{\partial^2 H}{\partial y^2} = \frac{1}{c_S^2}\ddot{H}, \tag{3}$$

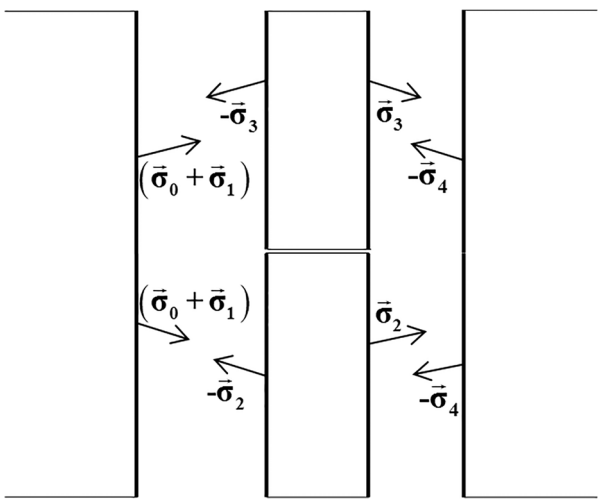

FIG. 3. Boundary conditions at the disbond.

where c_P and c_S are the wave speeds of pressure wave and shear waves, respectively. These must satisfy the zero-stress boundary condition at the top and bottom of the plate

$$\left.\begin{aligned}\sigma_{yy}\Big|_{(x<x_0-b;\ y=\pm h_1/2)} &= 0\\ \tau_{xy}\Big|_{(x<x_0-b;\ y=\pm h_1/2)} &= 0\end{aligned}\right\}\text{(Region 1)};\qquad \left.\begin{aligned}\sigma_{yy}\Big|_{(x_0+b>x>x_0-b;\ y=h_2-h_1/2,-h_1/2)} &= 0\\ \tau_{xy}\Big|_{(x_0+b>x>x_0-b;\ y=h_2-h_1/2,-h_1/2)} &= 0\end{aligned}\right\}\text{(Region 2)};$$

$$\left.\begin{aligned}\sigma_{yy}\Big|_{(x_0+b>x>x_0-b;\ y=h_1/2,h_2-h_1/2)} &= 0\\ \tau_{xy}\Big|_{(x_0+b>x>x_0-b;\ y=h_1/2,h_2-h_1/2)} &= 0\end{aligned}\right\}\text{(Region 3)};\qquad \left.\begin{aligned}\sigma_{yy}\Big|_{(x>x_0+b;\ y=\pm h_1/2)} &= 0\\ \tau_{xy}\Big|_{(x>x_0+b;\ y=\pm h_1/2)} &= 0\end{aligned}\right\}\text{(Region 4)}. \tag{4}$$

The stress and displacement field vectors associated with these wave fields are expressed as

$$\vec{\sigma} = \begin{bmatrix}\sigma_{xx}\\ \tau_{xy}\end{bmatrix};\quad \vec{u} = \begin{bmatrix}u_x\\ u_y\end{bmatrix}. \tag{5}$$

The boundary conditions at the horizontal crack are illustrated in Fig. 3. The boundary conditions at the interface at $x = x_0 - b$ are

$$(\vec{\sigma}_0 + \vec{\sigma}_1) = \begin{cases}\vec{\sigma}_3, & x = x_0 - b, \quad h_2 - h_1/2 \le y \le h_1/2\\ \vec{\sigma}_2, & x = x_0 - b, \quad -h_1/2 \le y \le h_2 - h_1/2,\end{cases} \tag{6}$$

$$\vec{u}_0 + \vec{u}_1 = \begin{cases}\vec{u}_3, & x = x_0 - b, \quad h_2 - h_1/2 \le y \le h_1/2\\ \vec{u}_2, & x = x_0 - b, \quad -h_1/2 \le y \le h_2 - h_1/2.\end{cases} \tag{7}$$

The boundary conditions at the interface at $x = x_0 + b$ are

$$\vec{\sigma}_4 = \begin{cases}\vec{\sigma}_3, & x = x_0 + b, \quad h_2 - h_1/2 \le y \le h_1/2\\ \vec{\sigma}_2, & x = x_0 + b, \quad -h_1/2 \le y \le h_2 - h_1/2,\end{cases} \tag{8}$$

$$\vec{u}_4 = \begin{cases}\vec{u}_3, & x = x_0 + b, \quad h_2 - h_1/2 \le y \le h_1/2\\ \vec{u}_2, & x = x_0 + b, \quad -h_1/2 \le y \le h_2 - h_1/2.\end{cases} \tag{9}$$

Subscript 0 stands for incident waves in Region 1, subscript 1 stands for reflected waves in Region 1, and subscripts 2 and 3 stand for the trapped waves in Regions 2 and 3, respectively. Subscript 4 stands for transmitted waves in Region 4. Let us assume the incident wave field in Region 1 to be harmonic of the form

$$\Phi_0 = f_0(y)e^{i(\xi_0 x - \omega t)}, \quad H_0 = ih_0(y)e^{i(\xi_0 x - \omega t)}, \tag{10}$$

where ξ_0 satisfies the Rayleigh-Lamb equation for Region 1, and $f_0(y)$, $h_0(y)$ are the corresponding wave modes.

C. Complex modes expansion of the scattered wave field

In this section, we present the general concept of our CMEP algorithm. We assume that the transmitted, reflected, and trapped wave fields have harmonic expressions similar to the incident wave field $(\Phi_0,\ H_0)$ given by Eq. (10). Since the boundary conditions at the horizontal crack cannot be satisfied by assuming any finite number of Lamb wave modes (Torvik, 1966), we expand these transmitted, reflected, and trapped wave fields in terms of all possible complex Lamb wave modes corresponding to the complex roots of Rayleigh-Lamb frequency equation with unknown complex amplitudes. Therefore, the scattered wave fields are expressed as

$$
\begin{aligned}
\Phi_1 &= \sum_{n_1=1}^{\infty} C_{1B,n_1}\Phi_{1B,n_1} = \sum_{n_1=1}^{\infty} C_{1B,n_1} f_{n_1}(y_1) e^{i(\xi_{1B,n_1}x-\omega t)}; \quad H_1 = \sum_{n_1=1}^{\infty} C_{1B,n_1} H_{1B,n_1} = \sum_{n_1=1}^{\infty} C_{1B,n_1} i h_{n_1}(y_1) e^{i(\xi_{1B,n_1}x-\omega t)};\\
\Phi_2 &= \sum_{n_2=1}^{\infty} (C_{2F,n_2}\Phi_{2F,n_2} + C_{2B,n_2}\Phi_{2B,n_2}) = \sum_{n_2=1}^{\infty} (C_{2F,n_2} f_{n_2}(y_2) e^{i(\xi_{2F,n_2}x-\omega t)} + C_{2B,n_2} f_{n_2}(y_2) e^{i(\xi_{2B,n_2}x-\omega t)});\\
H_2 &= \sum_{n_2=1}^{\infty} (C_{2F,n_2} H_{2F,n_2} + C_{2B,n_2} H_{2B,n_2}) = \sum_{n_2=1}^{\infty} (C_{2F,n_2} i h_{n_2}(y_2) e^{i(\xi_{2F,n_2}x-\omega t)} + C_{2B,n_2} i h_{n_2}(y_2) e^{i(\xi_{2B,n_2}x-\omega t)});\\
\Phi_3 &= \sum_{n_3=1}^{\infty} (C_{3F,n_3}\Phi_{3F,n_3} + C_{3B,n_3}\Phi_{3B,n_3}) = \sum_{n_3=1}^{\infty} (C_{3F,n_3} f_{n_3}(y_3) e^{i(\xi_{3F,n_3}x-\omega t)} + C_{3B,n_3} f_{n_3}(y_3) e^{i(\xi_{3B,n_3}x-\omega t)});\\
H_3 &= \sum_{n_3=1}^{\infty} (C_{3F,n_3} H_{3F,n_3} + C_{3B,n_3} H_{3B,n_3}) = \sum_{n_3=1}^{\infty} (C_{3F,n_3} i h_{n_3}(y_3) e^{i(\xi_{3F,n_3}x-\omega t)} + C_{3B,n_3} i h_{n_3}(y_3) e^{i(\xi_{3B,n_3}x-\omega t)});\\
\Phi_4 &= \sum_{n_4=1}^{\infty} C_{4F,n_4}\Phi_{4F,n_4} = \sum_{n_4=1}^{\infty} C_{4F,n_4} f_{n_4}(y_4) e^{i(\xi_{4F,n_4}x-\omega t)}; \quad H_4 = \sum_{n_4=1}^{\infty} C_{4F,n_4} H_{4F,n_4} = \sum_{n_4=1}^{\infty} C_{4F,n_4} i h_{n_4}(y_4) e^{i(\xi_{4F,n_4}x-\omega t)},
\end{aligned}
\tag{11}
$$

where subscripts B and F stand for backward and forward propagating wave, y_1, y_2, and y_3 are connected by the expressions $y_2 = y_1 + a_2$ and $y_3 = y_1 + a_3$ with $a_2 = (h_1 - h_2)/2$ and $a_3 = -h_2/2$ being the eccentricities of Region 2 and Region 3 from Region 1 and $y_1 = y_4$. The wavenumber ξ_{1B,n_1} is the (n_1)th complex root of the Rayleigh-Lamb equation corresponding to backward propagating Lamb waves in Region 1 and the wavenumbers ξ_{2F,n_2} and ξ_{2B,n_2} are (n_2)th complex root of the Rayleigh-Lamb equation corresponding to forward and backward propagating waves in Region 2, respectively. Similarly, wavenumber ξ_{4F,n_4} is the (n_4)th complex root of the Rayleigh-Lamb equation corresponding to forward propagating waves in Region 4 and the wavenumbers ξ_{3F,n_3} and ξ_{3B,n_3} are the (n_3)th complex roots of the Rayleigh-Lamb equation corresponding to forward and backward propagating waves in Region 3, respectively. The coefficient C_{1B,n_1} is the unknown amplitude of the (n_1)th mode of backward propagating Lamb waves in Region 1 whereas C_{2F,n_2} and C_{2B,n_2} are the unknown amplitudes of the (n_2)th mode of forward and backward propagating Lamb waves in Region 2, respectively. Similarly, the coefficient C_{4F,n_4} is the unknown amplitude of the (n_4)th mode of forward propagating Lamb waves in Region 4 whereas C_{3F,n_3} and C_{3B,n_3} are the unknown amplitudes of the (n_3)th mode of forward and backward propagating Lamb waves in Region 3, respectively. Equation (11) expresses the scattered wave field as the summation of all possible complex Lamb wave modes at a given frequency. The amplitudes C_{1B,n_1}, C_{2F,n_2}, C_{2B,n_2}, C_{3F,n_3}, C_{3B,n_3}, and C_{4F,n_4} of these modes have to be determined through the boundary matching process. Recall the boundary conditions at the interfaces at $x = x_0 - b$ and $x = x_0 + b$ are given by Eqs. (6), (7), (8), and (9). Also, note that the wave equations and the plate boundary conditions given by Eqs. (3) and (4) are satisfied by the definition of Lamb waves. We express the stress and displacement fields of Eqs. (6), (7), (8), and (9) using the complex Lamb wave mode expansion of Eq. (11), i.e.,

$$
\begin{aligned}
\vec{u}_1 &= \sum_{n_1=1}^{\infty} C_{1B,n_1} \begin{bmatrix} u_x \\ u_y \end{bmatrix}_{1B,n_1}; \quad \vec{\sigma}_1 = \sum_{n_1=1}^{\infty} C_{1B,n_1} \begin{bmatrix} \sigma_{xx} \\ \tau_{xy} \end{bmatrix}_{1B,n_1};\\
\vec{u}_2 &= \sum_{n_2=1}^{\infty} \left(C_{2F,n_2} \begin{bmatrix} u_x \\ u_y \end{bmatrix}_{2F,n_2} + C_{2B,n_2} \begin{bmatrix} u_x \\ u_y \end{bmatrix}_{2F,n_2} \right); \quad \vec{\sigma}_2 = \sum_{n_2=1}^{\infty} \left(C_{2F,n_2} \begin{bmatrix} \sigma_{xx} \\ \tau_{xy} \end{bmatrix}_{2F,n_2} + C_{2B,n_2} \begin{bmatrix} \sigma_{xx} \\ \tau_{xy} \end{bmatrix}_{2F,n_2} \right);\\
\vec{u}_3 &= \sum_{n_3=1}^{\infty} \left(C_{3F,n_3} \begin{bmatrix} u_x \\ u_y \end{bmatrix}_{3F,n_3} + C_{3B,n_3} \begin{bmatrix} u_x \\ u_y \end{bmatrix}_{3F,n_3} \right); \quad \vec{\sigma}_3 = \sum_{n_3=1}^{\infty} \left(C_{3F,n_3} \begin{bmatrix} \sigma_{xx} \\ \tau_{xy} \end{bmatrix}_{3F,n_3} + C_{3B,n_3} \begin{bmatrix} \sigma_{xx} \\ \tau_{xy} \end{bmatrix}_{3F,n_3} \right);\\
\vec{u}_4 &= \sum_{n_4=1}^{\infty} C_{4F,n_4} \begin{bmatrix} u_x \\ u_y \end{bmatrix}_{4F,n_4}; \quad \vec{\sigma}_4 = \sum_{n_4=1}^{\infty} C_{4F,n_4} \begin{bmatrix} \sigma_{xx} \\ \tau_{xy} \end{bmatrix}_{4F,n_4}.
\end{aligned}
\tag{12}
$$

In the same vein, the incident wave field uses subscript 0, i.e.,

$$
\vec{u}_0 = \begin{bmatrix} u_x \\ u_y \end{bmatrix}_0, \quad \vec{\sigma}_0 = \begin{bmatrix} \sigma_{xx} \\ \tau_{xy} \end{bmatrix}_0.
\tag{13}
$$

Next, we use the complex modes expansion of these wave fields to express the boundary conditions at the horizontal crack. Therefore, using Eqs. (12) and (13) into Eqs. (6), (7), (8), and (9) yields

$$
\vec{\sigma}_0 + \vec{\sigma}_1 = \begin{cases} \vec{\sigma}_3, & x = x_0 - b, \quad h_2 - h_1/2 \le y \le h_1/2 \\ \vec{\sigma}_2, & x = x_0 - b, \quad -h_1/2 \le y \le h_2 - h_1/2, \end{cases}
\tag{14}
$$

$$\vec{u}_0 + \vec{u}_1 = \vec{u}_3, \quad x = x_0 - b, \quad h_2 - h_1/2 \le y \le h_1/2, \tag{15}$$

$$\vec{u}_0 + \vec{u}_1 = \vec{u}_2, \quad x = x_0 - b, \quad -h_1/2 \le y \le h_2 - h_1/2, \tag{16}$$

$$\vec{\sigma}_4 = \begin{cases} \vec{\sigma}_3, & x = x_0 + b, \quad h_2 - h_1/2 \le y \le h_1/2 \\ \vec{\sigma}_2, & x = x_0 + b, \quad -h_1/2 \le y \le h_2 - h_1/2, \end{cases} \tag{17}$$

$$\vec{u}_4 = \vec{u}_3, \quad x = x_0 + b, \quad h_2 - h_1/2 \le y \le h_1/2, \tag{18}$$

$$\vec{u}_4 = \vec{u}_2, \quad x = x_0 + b, \quad -h_1/2 \le y \le h_2 - h_1/2. \tag{19}$$

Therefore, Eqs. (14), (15), (16), (17), (18), and (19) represent the thickness dependent boundary conditions at the horizontal crack expressed using complex modes expansion of Lamb waves.

D. Vector projection of the boundary conditions

To make Eqs. (14), (15), (17), and (18) independent of y, we follow Grahn (2003) and project them onto appropriate complete orthogonal vector spaces. But, different from Grahn (2003), we do not use generic sine and cosine functions, instead we use the time averaged power flow expression which uses the stress-velocity product (Auld, 1973). Thus, in Region 1, we project the stress boundary conditions (14), onto the conjugate displacement vector space of the complex Lamb wave modes; in Regions 2 and 3, we project the displacement boundary conditions (15), (16), (18), and (19), onto the conjugate stress vector space of the complex Lamb wave modes. By the same token, in Region 4, we project the stress boundary conditions (17), onto the conjugate displacement vector space of the complex Lamb wave modes. By doing so, the CMEP formulation incorporates the average power flow associated with the reflected, transmitted, and trapped wave fields.

The projection vector space for Eq. (14) is

$$\vec{\bar{u}}_{1B} = \text{conj}\begin{bmatrix} u_x \\ u_y \end{bmatrix}_{1B,\bar{n}_1} = \begin{bmatrix} \bar{u}_x \\ \bar{u}_y \end{bmatrix}_{1B,\bar{n}_1}, \quad \bar{n}_1 = 1, 2, 3, ... \tag{20}$$

After projecting Eq. (14) onto Eq. (20), the stress boundary conditions in Eq. (14) take the form

$$\begin{aligned} \int_{-h_1/2}^{h_1/2} (\vec{\sigma}_0 + \vec{\sigma}_1) \cdot \vec{\bar{u}}_{1B} dy = \int_{-h_1/2}^{h_2-h_1/2} \vec{\sigma}_2 \cdot \vec{\bar{u}}_{1B} dy + \int_{h_2-h_1/2}^{h_1/2} \vec{\sigma}_3 \cdot \vec{\bar{u}}_{1B} dy \\ \Rightarrow \sum_{n_2=1}^{\infty} \left(C_{2F,n_2} \left\langle \begin{bmatrix} \sigma_{xx} \\ \tau_{xy} \end{bmatrix}_{2F,n_2}, \begin{bmatrix} \bar{u}_x \\ \bar{u}_y \end{bmatrix}_{1B,\bar{n}_1} \right\rangle_{-h_1/2}^{h_2-h_1/2} + C_{2B,n_2} \left\langle \begin{bmatrix} \sigma_{xx} \\ \tau_{xy} \end{bmatrix}_{2B,n_2}, \begin{bmatrix} \bar{u}_x \\ \bar{u}_y \end{bmatrix}_{1B,\bar{n}_1} \right\rangle_{-h_1/2}^{h_2-h_1/2} \right) \\ + \sum_{n_3=1}^{\infty} \left(C_{3F,n_3} \left\langle \begin{bmatrix} \sigma_{xx} \\ \tau_{xy} \end{bmatrix}_{3F,n_3}, \begin{bmatrix} \bar{u}_x \\ \bar{u}_y \end{bmatrix}_{1B,\bar{n}_1} \right\rangle_{h_2-h_1/2}^{h_1/2} + C_{3B,n_3} \left\langle \begin{bmatrix} \sigma_{xx} \\ \tau_{xy} \end{bmatrix}_{3B,n_3}, \begin{bmatrix} \bar{u}_x \\ \bar{u}_y \end{bmatrix}_{1B,\bar{n}_1} \right\rangle_{h_2-h_1/2}^{h_1/2} \right) \\ - \sum_{n_1=1}^{\infty} C_{1B,n_1} \left\langle \begin{bmatrix} \sigma_{xx} \\ \tau_{xy} \end{bmatrix}_{1B,n_1}, \begin{bmatrix} \bar{u}_x \\ \bar{u}_y \end{bmatrix}_{1B,\bar{n}_1} \right\rangle_{-h_1/2}^{h_1/2} = \left\langle \begin{bmatrix} \sigma_{xx} \\ \tau_{xy} \end{bmatrix}_0, \begin{bmatrix} \bar{u}_x \\ \bar{u}_y \end{bmatrix}_{1B,\bar{n}_1} \right\rangle_{-h_1/2}^{h_1/2}; \quad n_1, n_2, n_3 = 1, 2, 3, ..., \end{aligned} \tag{21}$$

where $\int_a^b P \cdot Q dy = \langle P, Q \rangle_a^b$ represents the inner product. Note that this projection incorporates the power flow expression associated with the reflected modes. Also, to incorporate the power flow expression associated with the transmitted modes we choose the projection vector space for Eq. (17) as

$$\vec{\bar{u}}_{4F} = \text{conj}\begin{bmatrix} u_x \\ u_y \end{bmatrix}_{4F,\bar{n}_4} = \begin{bmatrix} \bar{u}_x \\ \bar{u}_y \end{bmatrix}_{4F,\bar{n}_4}, \quad \bar{n}_4 = 1, 2, 3, ... \tag{22}$$

Similarly, to incorporate the power flow expressions associated with forward and backward propagating modes in Regions 2 and 3 we choose the projection vector spaces for Eqs. (16), (19), (15), and (18) as

$$\vec{\bar{\sigma}}_{2F} = \text{conj}\begin{bmatrix} \sigma_{xx} \\ \tau_{xy} \end{bmatrix}_{2F,\bar{n}_2} = \begin{bmatrix} \bar{\sigma}_{xx} \\ \bar{\tau}_{xy} \end{bmatrix}_{2F,\bar{n}_2}, \quad \bar{n}_2 = 1, 2, 3, ..., \tag{23}$$

$$\vec{\bar{\sigma}}_{2B} = \text{conj}\begin{bmatrix} \sigma_{xx} \\ \tau_{xy} \end{bmatrix}_{2B,\bar{n}_2} = \begin{bmatrix} \bar{\sigma}_{xx} \\ \bar{\tau}_{xy} \end{bmatrix}_{2B,\bar{n}_2}, \quad \bar{n}_2 = 1, 2, 3, ..., \tag{24}$$

$$\vec{\bar{\sigma}}_{3F} = \text{conj}\begin{bmatrix} \sigma_{xx} \\ \tau_{xy} \end{bmatrix}_{3F,\bar{n}_3} = \begin{bmatrix} \bar{\sigma}_{xx} \\ \bar{\tau}_{xy} \end{bmatrix}_{3F,\bar{n}_3}, \quad \bar{n}_3 = 1, 2, 3, ..., \tag{25}$$

$$\vec{\bar{\sigma}}_{3B} = \text{conj}\begin{bmatrix} \sigma_{xx} \\ \tau_{xy} \end{bmatrix}_{3B,\bar{n}_3} = \begin{bmatrix} \bar{\sigma}_{xx} \\ \bar{\tau}_{xy} \end{bmatrix}_{3B,\bar{n}_3}, \quad \bar{n}_3 = 1, 2, 3, ... \tag{26}$$

This method of projection for a horizontal crack transforms the stress and displacement equations into power flow equations incorporating power flow expressions for scattered wave fields in all the wave guides.

E. Numerical solution

For numerical calculation we consider finite values for the indices n_1, n_2, n_3, n_4, $\bar{n}_1$, $\bar{n}_2$, $\bar{n}_3$, $\bar{n}_4$. We assume $n_1 = 1, 2, 3, ..., N_1$, $n_2 = 1, 2, 3, ..., N_2$, $n_3 = 1, 2, 3, ..., N_3$, $n_4 = 1, 2, 3, ..., N_4$, $\bar{n}_1 = 1, 2, 3, ..., \bar{N}_1$, $\bar{n}_2 = 1, 2, 3, ..., \bar{N}_2$, $\bar{n}_3 = 1, 2, 3, ..., \bar{N}_3$, $\bar{n}_4 = 1, 2, 3, ..., \bar{N}_4$. Recall that the $(N_1 + 2N_2 + 2N_3 + N_4)$ unknowns are the complex Lamb wave mode amplitudes $(C_{1B,n_1}, C_{2F,n_2}, C_{2B,n_2}, C_{3F,n_3}, C_{3B,n_3}, C_{4F,n_4})$. Thus, after performing the projection operations, Eqs. (14), (15), (16), (17), (18), and (19) form a set of $(\bar{N}_1 + 2\bar{N}_2 + 2\bar{N}_3 + \bar{N}_4)$ linear algebraic equations in $(N_1 + 2N_2 + 2N_3 + N_4)$ unknowns C_{1B,n_1}, C_{2F,n_2}, C_{2B,n_2}, C_{3F,n_3}, C_{3B,n_3}, C_{4F,n_4}. By assuming $N_1 = N_2 = N_3 = N_4 = \bar{N}_1 = \bar{N}_2 = \bar{N}_3 = \bar{N}_4 = N$, we get $6N$ equations in $6N$ unknowns. Then final system of equations can be written as

$$[A]_{N\times N}\{C_{2F}\}_{N\times 1} + [B]_{N\times N}\{C_{2B}\}_{N\times 1} + [D]_{N\times N}\{C_{3F}\}_{N\times 1} + [E]_{N\times N}\{C_{3B}\}_{N\times 1} - [F]_{N\times N}\{C_{1B}\}_{N\times 1} - [0]_{N\times N}\{C_{4F}\}_{N\times 1} = \{G\}_{N\times 1}, \tag{27}$$

$$[H]_{N\times N}\{C_{2F}\}_{N\times 1} + [J]_{N\times N}\{C_{2B}\}_{N\times 1} + [K]_{N\times N}\{C_{3F}\}_{N\times 1} + [L]_{N\times N}\{C_{3B}\}_{N\times 1} - [0]_{N\times N}\{C_{1B}\}_{N\times 1} - [M]_{N\times N}\{C_{4F}\}_{N\times 1} = \{0\}_{N\times 1}, \tag{28}$$

$$[0]_{N\times N}\{C_{2F}\}_{N\times 1} + [0]_{N\times N}\{C_{2B}\}_{N\times 1} + [N]_{N\times N}\{C_{3F}\}_{N\times 1} + [O]_{N\times N}\{C_{3B}\}_{N\times 1} - [P]_{N\times N}\{C_{1B}\}_{N\times 1} - [0]_{N\times N}\{C_{4F}\}_{N\times 1} = \{Q\}_{N\times 1}, \tag{29}$$

$$[R]_{N\times N}\{C_{2F}\}_{N\times 1} + [S]_{N\times N}\{C_{2B}\}_{N\times 1} + [0]_{N\times N}\{C_{3F}\}_{N\times 1} + [0]_{N\times N}\{C_{3B}\}_{N\times 1} - [T]_{N\times N}\{C_{1B}\}_{N\times 1} - [0]_{N\times N}\{C_{4F}\}_{N\times 1} = \{U\}_{N\times 1}, \tag{30}$$

$$[0]_{N\times N}\{C_{2F}\}_{N\times 1} + [0]_{N\times N}\{C_{2B}\}_{N\times 1} + [V]_{N\times N}\{C_{3F}\}_{N\times 1} + [W]_{N\times N}\{C_{3B}\}_{N\times 1} - [0]_{N\times N}\{C_{1B}\}_{N\times 1} - [X]_{N\times N}\{C_{4F}\}_{N\times 1} = \{0\}_{N\times 1}, \tag{31}$$

$$[Y]_{N\times N}\{C_{2F}\}_{N\times 1} + [Z]_{N\times N}\{C_{2B}\}_{N\times 1} + [0]_{N\times N}\{C_{3F}\}_{N\times 1} + [0]_{N\times N}\{C_{3B}\}_{N\times 1} - [0]_{N\times N}\{C_{1B}\}_{N\times 1} - [\Gamma]_{N\times N}\{C_{4F}\}_{N\times 1} = \{0\}_{N\times 1}. \tag{32}$$

In Eqs. (27), (28), (29), (30), (31), and (32) the coefficient matrices $[A]$, $[B]$, $[D]$, $[E]$, $[F]$, $[G]$, $[H]$, $[J]$, $[K]$, $[L]$, $[M]$, $[N]$, $[O]$, $[P]$, $[Q]$, $[R]$, $[S]$, $[T]$, $[U]$, $[V]$, $[W]$, $[X]$, $[Y]$, $[Z]$, and $[\Gamma]$ are known matrices containing the vector-projected boundary conditions; the vectors $\{C_{2F}\}$, $\{C_{2B}\}$, $\{C_{3F}\}$, $\{C_{3B}\}$, $\{C_{1B}\}$, and $\{C_{4F}\}$ contain the unknown coefficients. Combining Eqs. (27)–(32) yields

$$\begin{bmatrix} A & B & D & E & -F & 0 \\ H & J & K & L & 0 & -M \\ 0 & 0 & N & O & -P & 0 \\ R & S & 0 & 0 & -T & 0 \\ 0 & 0 & V & W & 0 & -X \\ Y & Z & 0 & 0 & 0 & -\Gamma \end{bmatrix}_{6N\times 6N} \begin{Bmatrix} C_{2F} \\ C_{2B} \\ C_{3F} \\ C_{3B} \\ C_{1B} \\ C_{4F} \end{Bmatrix}_{6N\times 1} = \begin{Bmatrix} G \\ 0 \\ Q \\ U \\ 0 \\ 0 \end{Bmatrix}_{6N\times 1} \Rightarrow [\Upsilon]_{6N\times 6N}\{C\}_{6N\times 1} = \{\Lambda\}_{6N\times 1}. \tag{33}$$

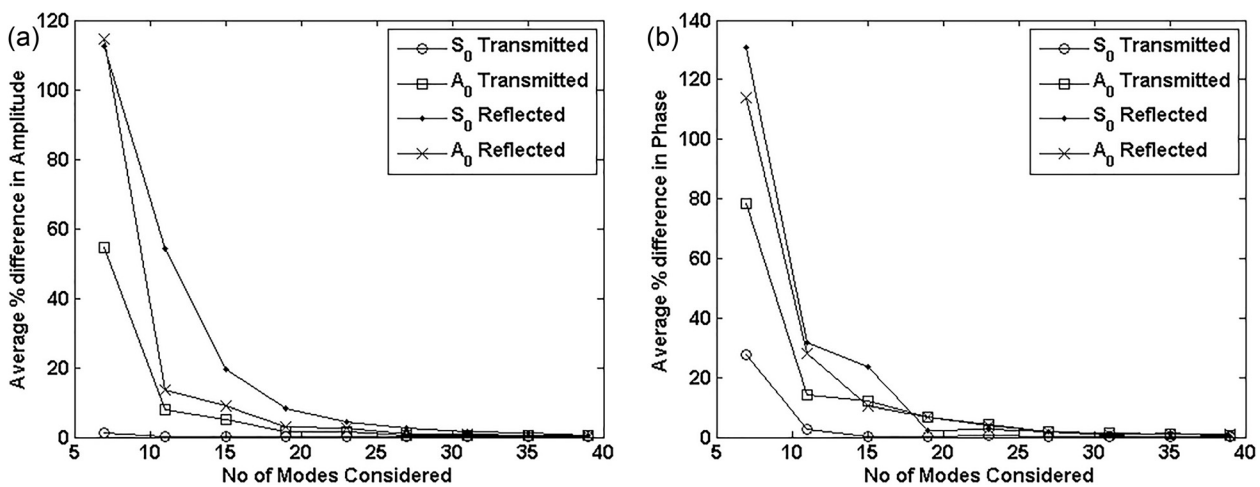

FIG. 4. Convergence of (a) amplitudes, (b) phases of scattered Lamb wave modes for S0 mode incident on a disbond with $R_d = 0.25$ and $R_w = 5$; results are averaged over a wide frequency range, 200 kHz mm to 1.5 MHz mm.

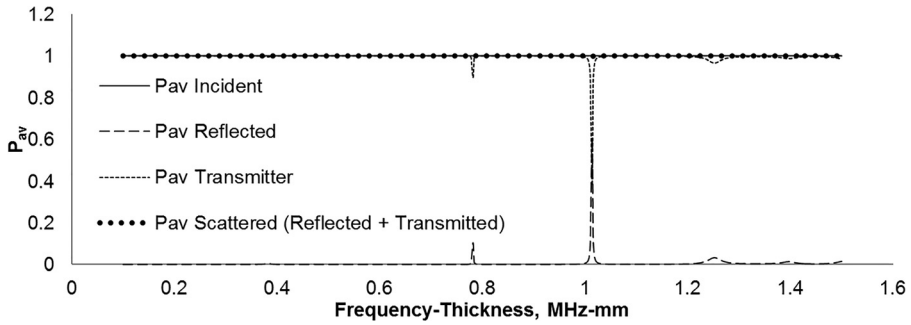

FIG. 5. Variation of time average power flow P_{av} through the disbond as calculated by CMEP with a 39-mode expansion (S0 mode incident on a disbond with $R_d = 0.25$ and $R_w = 5$).

Equation (33) can be solved for the unknown amplitudes of the reflected and transmitted Lamb wave modes as

$$\{C\}_{6N\times 1} = [\Upsilon]^{-1}_{6N\times 6N}[\Lambda]_{6N\times 1}. \tag{34}$$

As a test case we consider a horizontal crack in an aluminum plate with $E = 70$ GPa, $\rho = 2780$ kg/m^3, $\nu = 0.33$, $h_1 = 2$ mm, $h_2 = 1.5$ mm, and $b = 5$ mm. This results in a depth ratio $R_d = (h_1 - h_2)/h_1 = 0.25$, and a width ratio $R_w = 2b/h_1 = 5$. We also consider S0 as the incident Lamb wave mode. We use a frequency range of up to 1.5 MHz mm for its relevance to practical applications. We perform convergence studies to determine the maximum number of complex roots of the Rayleigh-Lamb equation needed to calculate the first two scattered Lamb wave modes with high accuracy. Figure 4 shows the convergence study for the amplitudes of the first two modes of Lamb waves, S0 and A0. Considering 39 modes in the expansion ensured convergence to about 0.5% error. Another important verification of convergence is the power flow balance. Figure 5 shows that a 39-mode expansion gave a balanced average power flow though the vertical horizontal cracks over the whole frequency range up to 750 kHz. It is apparent that power flow balance requirements are met since the "P_{av} incident" line exactly overlaps with the "P_{av} Scattered (Reflected + Transmitted)" line. Also, Fig. 5 shows that at certain frequencies the power flow associated with reflected and transmitted waves show sharp spikes. This is because the forward and backward propagating trapped Lamb wave modes in Regions 2 and 3 form standing wave fields between the two geometric interfaces of the horizontal crack and at these frequencies the standing wave modes resonates and increases scattered wave amplitudes as well. Similar behavior was also shown by Glushkov *et al.* (2009) for notch type damages.

III. VERIFICATION OF THE MODEL

A. FEM simulation strategy

For the verification of the results from CMEP at higher frequencies, we made finite element models using commercial software ANSYS. The dimensions and material properties were chosen as described in Sec. II E. The frequency range for comparison was chosen to be 50–750 kHz to avoid exciting A1 and other higher propagating modes. To achieve accuracy, PLANE182 element with 0.08 mm length was chosen. This resulted in $\lambda/l_{FEM} \geq 30$ (Fig. 6) which is higher than the recommended value for an accurate result (Moser *et al.*, 1999).

We performed harmonic analysis in ANSYS to verify the CMEP results in the frequency domain. To achieve a transient response from a finite dimensional model by harmonic analysis, we introduced non-reflective boundaries (NRBs) at both the ends of the model to eliminate the boundary reflections and thereby eliminating the possibility of standing waves (Fig. 7). The NRBs were created using the COMBIN14 spring damper element (Shen and Giurgiutiu, 2015). These elements were arranged at the top and bottom surfaces of the NRBs and also at both ends. The damping coefficients of the elements were varied gradually in a sinusoidal pattern starting from zero (Fig. 7). This eliminated any reflection from the edge of the NRB itself. The incident S0 wave was generated by exciting the top and bottom nodes simultaneously at the transmission location. The scattered waves were detected at the top and bottom nodes of the sensing locations in Region 1 and Region 2.

A similar model was created without the horizontal crack to capture the incident wave field only. We subtracted the incident wave field from the wave field at Region 1 obtained from the horizontal crack model to get the reflected wave fields. The transmitted wave field was obtained directly from Region 2.

At the given frequencies of excitation there are only S0 and A0 modes as propagating modes of Lamb waves. Since the sensing locations are at sufficient distances from the damage as well as source, amplitudes of all the evanescent modes decay almost entirely (99.999 999%) before they reach the sensing locations. Therefore, the sensed scattered

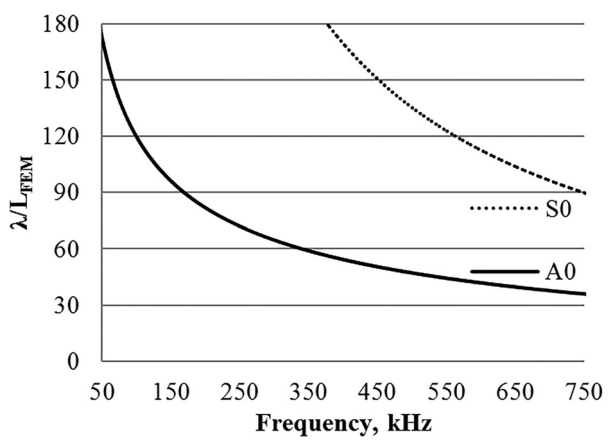

FIG. 6. Variation of λ/l_{FEM} with frequency.

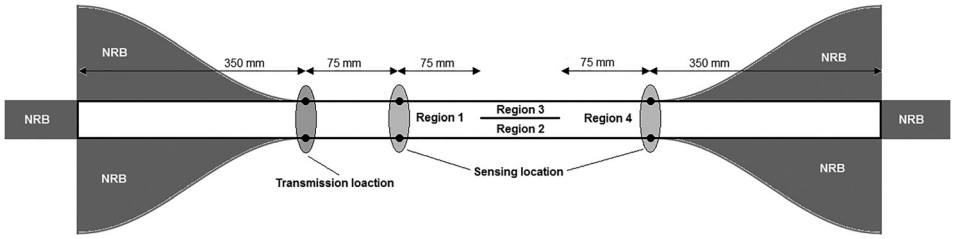

FIG. 7. Schematics of the finite element model with nonreflecting boundary for harmonic analysis.

wave fields contain only propagating Lamb wave modes. To obtain the in-plane displacement component for the symmetric mode, we averaged the sum of in-plane displacements extracted at the top and bottom nodes; for the antisymmetric mode, we averaged the subtraction of in-plane displacements extracted at the top and bottom nodes. This method works because S0 contains in-plane type motion and A0 contains out-of-plane type.

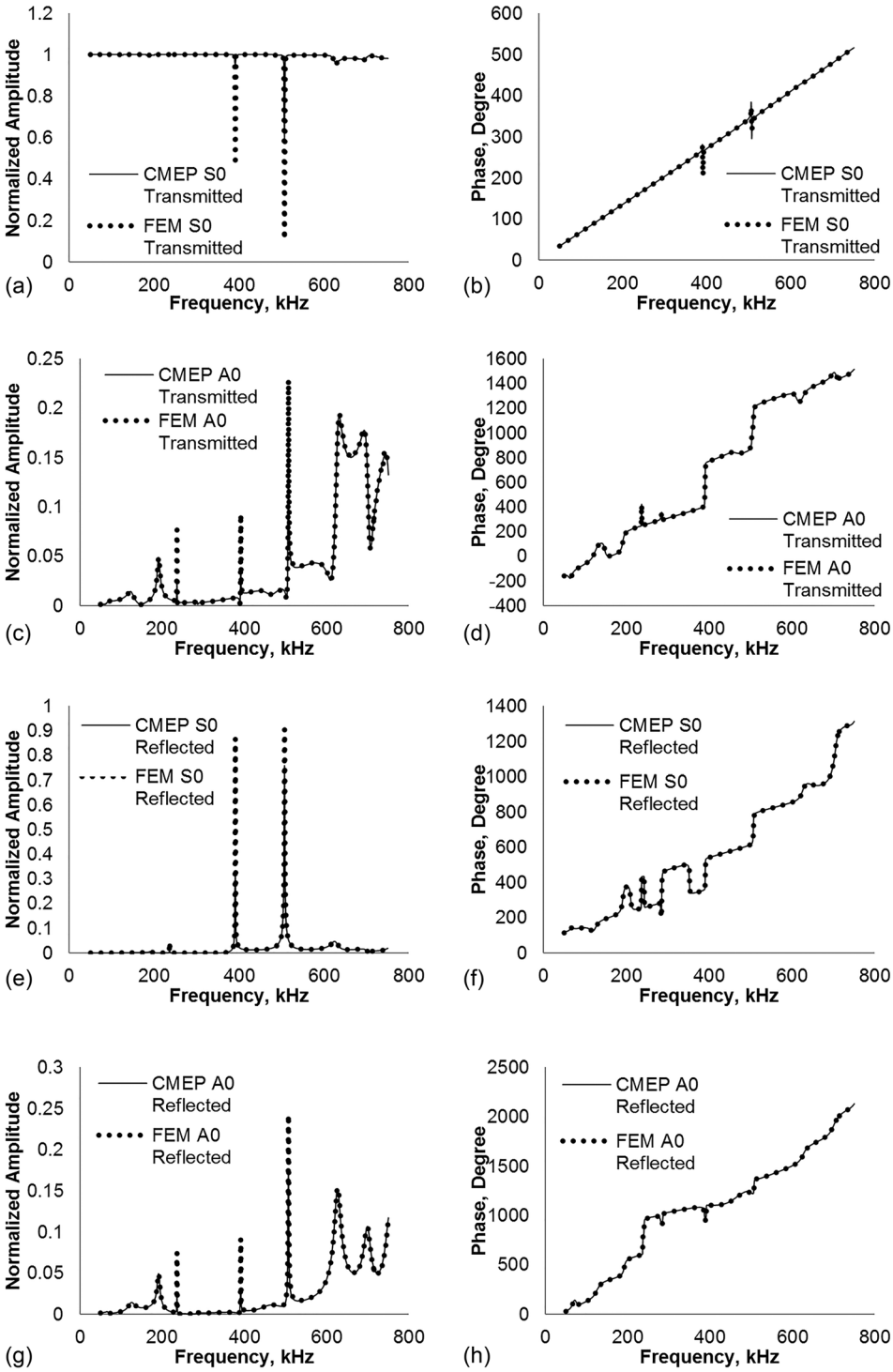

FIG. 8. Comparison of u_x displacement of (a) transmitted S0 mode amplitude, (b) transmitted S0 mode phase, (c) transmitted A0 mode amplitude, (d) transmitted A0 mode phase, (e) reflected S0 mode amplitude, (f) reflected S0 mode phase, (g) reflected A0 mode amplitude, and (h) reflected A0 mode phase for incident S0 mode scattered from a disbond with $R_d = 0.25$ and $R_w = 5$.

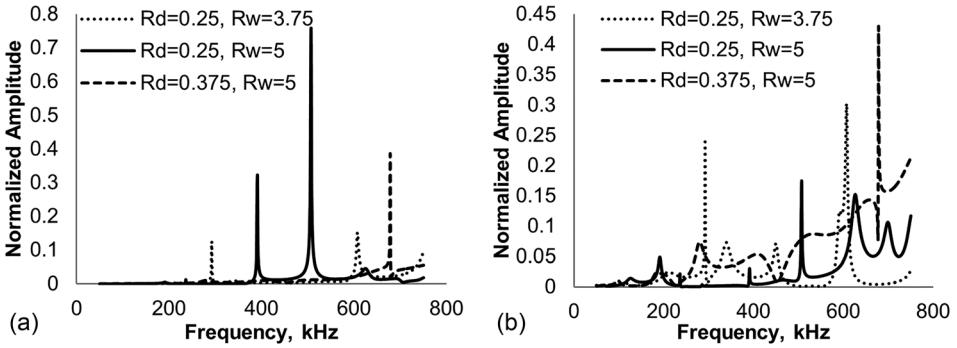

FIG. 9. Comparison of u_x displacement of (a) reflected S0 mode amplitude and (b) reflected A0 mode phase for different values of R_d and R_w.

B. Comparison of CMEP and FEM results

Figure 8 shows the comparison of results from CMEP and FEM; we can see that the amplitudes and phases of the reflected and transmitted waves obtained from FEM are convergent with the CMEP results for a wide range of frequencies. Both CMEP and FEM results show characteristic resonances of the horizontal crack at certain frequencies due to the standing wave field created by trapped Lamb wave modes. As shown in Fig. 9, these resonance frequencies depend on length and depth of the horizontal crack. Therefore these frequencies can be used to determine the lengths and depths of horizontal cracks and disbonds.

However, the convergence of finite element models is quite expensive in terms of computational time; FEM takes about 200 times more computational time than CMEP to compute the same results. This disparity in computational time is due to the fact that FEM requires very fine discretization for convergence of both phase and amplitude. It is very important to obtain correct scatter coefficients quickly for NDE and SHM. Therefore, with fast, accurate, and reliable prediction of the scatter field, CMEP can be an important tool to solve the inverse problem of detection and characterization of horizontal cracks and disbonds.

IV. SUMMARY, CONCLUSION, AND FUTURE WORK

A. Summary

In this study, we demonstrated a stable and robust algorithm for analyzing the interaction between Lamb waves and a horizontal crack using the CMEP approach. First, we used the complex Lamb wave modes to express the scatter field solution as a wave modes expansion. Next, we formulated the boundary condition at the geometric interfaces in terms of tractions and displacements continuity which resulted in a set of 16 thickness dependent boundary conditions. This thickness dependence was eliminated by using the complex power flow associated with Lamb wave modes; we used vector projection of the displacement equations onto the conjugate stresses and the stress equations onto the conjugate displacements. This process resulted in an infinite set of complex-valued linear algebraic equations which was truncated to finite sizes. The truncated system was solved for the unknown scattered wave amplitudes. A convergence study was performed considering only the propagating modes; it was found that approximately 39 modes are sufficient to obtain less than 0.5% convergence. The CMEP predictions were compared with FEM results at a wide frequency range. It was found that FEM results agree with the CMEP results but at a much higher computational cost. Conversely, the CMEP algorithm described in this paper is orders of magnitude faster than the FEM approach for similar order of accuracy. As a by-product, the CMEP method also yields the local vibration field trapped at the damage which involves the complex evanescent wave modes. However, for accuracy of this prediction a convergence study concerning the trapped complex evanescent modes needs to be performed.

B. Conclusion

We demonstrated that the full Lamb wave complex eigen-space can be used efficiently to project the interface boundary conditions for a normal modes representation of the scattered field in the case of a horizontal crack or disbond. We demonstrated that CMEP can capture the reflected and transmitted wave amplitudes as accurately as FEM. We have also shown that both CMEP and FEM can capture the characteristic resonance of horizontal cracks. However, for FEM the accuracy of the results requires higher discretization with a much higher computational cost at higher frequencies (Moser *et al.*, 1999). The same calculations can be done using CMEP in significantly lower computation time. At high frequencies, when many propagating Lamb wave modes exist, CMEP is a better choice than FEM because it permits the accurate and reliable computation of individual amplitudes and phases of the many reflected and transmitted modes.

ACKNOWLEDGMENTS

Support from the Office of Naval Research # N00014-11-1-0271, Dr. Ignacio Perez, Program Officer, the Air Force Office of Scientific Research #FA9550-11-1-0133, and Dr. David Stargel, Program Manager, are thankfully acknowledged.

Auld, B. A. (**1973**). *Acoustic Fields and Waves in Solids*, Vol. II (Wiley, New York), pp. 1–414.

Castaings, M., Le Clezio, E., and Hosten, B. (**2002**). "Modal decomposition method for modeling the interaction of Lamb waves with cracks," J. Acoust. Soc. Am. **112**(6), 2567–2582.

Cho, Y., and Rose, J. L. (**2000**). "An elastodynamic hybrid boundary element study for elastic guided wave interactions with a surface breaking defect," Int. J. Solids Struct. **37**(30), 4103–4124.

Diligent, O., Lowe, M. J. S., Le Clézio, E., Castaings, M., and Hosten, B. (**2003**). "Prediction and measurement of nonpropagating Lamb modes at the free end of a plate when the fundamental antisymmetric mode A0 is incident," J. Acoust. Soc. Am. **113**(6), 3032–3042.

Flores-López, M. A., and Gregory, R. D. (**2006**). "Scattering of Rayleigh-Lamb waves by a surface breaking crack in an elastic plate," J. Acoust. Soc. Am. **119**(4), 2041–2049.
Galán, J. M., and Abascal, R. (**2005**). "Lamb mode conversion at edges. A hybrid boundary element-finite-element solution," J. Acoust. Soc. Am. **117**(4), 1777–1784.
Glushkov, Y. V., Glushkova, N. V., Yeremin, A. A., and Mikhas'kiv, V. V. (**2009**). "The layered element method in the dynamic theory of elasticity," J. Appl. Math. Mech. **73**(4), 449–456.
Grahn, T. (**2003**). "Lamb wave scattering from a circular partly through-thickness hole in a plate," Wave Motion **37**(1), 63–80.
Gregory, R. D., and Gladwell, I. (**1982**). "The cantilever beam under tension, bending or flexure at infinity," J. Elast. **12**(4), 317–343.
Gregory, R. D., and Gladwell, I. (**1983**). "The reflection of a symmetric Rayleigh-Lamb wave at the fixed or free edge of a plate," J. Elast. **13**, 185–206.
Gunawan, A., and Hirose, S. (**2004**). "Mode-exciting method for Lamb wave-scattering analysis," J. Acoust. Soc. Am. **115**(3), 996–1005.
Hull, A. J., and Maguire, J. M. (**2014**). "Elastic response of an orthogonally reinforced plate," J. Sound Vib. **333**(8), 2327–2346.
Hull, A. J., and Welch, J. R. (**2010**). "Elastic response of an acoustic coating on a rib-stiffened plate," J. Sound Vib. **329**(20), 4192–4211.
Karim, M. R., Awal, M. A., and Kundu, T. (**1992**). "Elastic wave scattering by cracks and inclusions in plates: In-plane case," Int. J. Solids Struct. **29**(19), 2355–2367.
Lamb, H. (**1917**). "On waves in an elastic plate," Proc. R. Soc. **93**(648), 114–128.
Lampman, S. R., Zorc, T. B., and Ronke, A. W. (editors). (**1989**). *ASM Handbook, Vol. 17: Nondestructive Evaluation and Quality Control* (ASM International), pp. 489–609, available at http://products.asminternational.org/hbk/index.jsp.
Mackerle, J. (**2004**). "Finite-element modelling of non-destructive material evaluation, an addendum: A bibliography (1997–2003)," Model. Simul. Mater. Sci. Eng. **12**, 799–834.
Moreau, L., Caleap, M., Velichko, A., and Wilcox, P. D. (**2011**). "Scattering of guided waves by through-thickness cavities with irregular shapes," Wave Motion **48**(7), 586–602.
Moreau, L., Caleap, M., Velichko, A., and Wilcox, P. D. (**2012**). "Scattering of guided waves by flat-bottomed cavities with irregular shapes," Wave Motion **49**(2), 375–387.
Morvan, B., Wilkie-Chancellier, N., Duflo, H., Tinel, A., and Duclos, J. (**2003**). "Lamb wave reflection at the free edge of a plate," J. Acoust. Soc. Am. **113**(3), 1417–1425.
Moser, F., Jacobs, L. J., and Qu, J. (**1999**). "Modeling elastic wave propagation in waveguides with the finite element method," NDT & E Int. **32**(4), 225–234.
Rokhlin, S. (**1980**). "Diffraction of Lamb waves by a finite crack in an elastic layer," J. Acoust. Soc. Am. **67**(4), 1157–1165.
Shen, Y., and Giurgiutiu, V. (**2015**). "Effective non-reflective boundary for Lamb waves: Theory, finite element implementation, and applications," Wave Motion **58**, 22–41.
Terrien, N., Osmont, D., Royer, D., Lepoutre, F., and Déom, A. (**2007**). "A combined finite element and modal decomposition method to study the interaction of Lamb modes with micro-defects," Ultrasonics **46**(1), 74–88.
Torvik, P. J. (**1966**). "Reflection of wave trains in semi-infinite plates," J. Acoust. Soc. Am. **41**(2), 346–353.
Wang, C. H., and Rose, L. R. F. (**2003**). "Wave reflection and transmission in beams containing delamination and inhomogeneity," J. Sound Vib. **264**(4), 851–872.